$Ag_{10}Te_4Br_3$: A New Silver(I) (poly)Chalcogenide Halide Solid Electrolyte

Stefan Lange and Tom Nilges*

Institut für Anorganische und Analytische Chemie, Universität Münster, Corrensstrasse 30, D-48149 Münster, Germany

Received January 28, 2006. Revised Manuscript Received March 10, 2006

$Ag_{10}Te_4Br_3$ is the first representative of an M(group 11) (poly)chalcogenide halide with covalently bonded $[Te_2]^{2-}$ units and isolated Te^{2-} ions. It represents a new class of materials located between M(group 11) chalcogen halides, characterized by covalently bonded chalcogen structure motives, on the one hand and chalcogenide halides, consisting of isolated chalcogenide ions, on the other. A high silver mobility on distinct silver layers was observed for orthorhombic $Ag_{10}Te_4Br_3$, resulting in a pronounced 1D silver mobility at room temperature. The covalent regions of the chalcogen substructure account for the lowest activation energies, determined after a detailed analysis of the silver joint probability density functions (jpdf). Impedance spectroscopic measurements were performed in order to substantiate the results from jpdf analyses. $Ag_{10}Te_4Br_3$ is an excellent conductor, with conductivities on the same order of magnitude as β-Ag_3SX (X = I, Br) or glassy silver chalcogenide halides. The occurrence of the $[Te_2]^{2-}$ dumbbell was substantiated by Raman spectroscopy.

1. Introduction

Materials showing optimized electric and magnetic properties are playing a crucial role in today's high-technology applications such as sensors, batteries, microelectronics, and semiconductor devices.[1−6] Ongoing scientific progress, especially in the fields of microelectronics and consumer electronics, is of general interest. Silver(I) chalcogenide halides and silver(I) chalcogenides are potential candidates for contribution to this progress because of their physical properties, including high ion conductivity (Ag_3SX with X = I, Br; Ag_5Te_2Cl)[7−11] or colossal magnetoresistance (Ag_2Q with Q = Te, Se).[12−14] A promising and rapidly increasing field for silver-containing solid electrolytes is the development of nonvolatile memory devices. So-called programmable metallization cell memory devices (PMC) are based on the electrochemical generation of nanosized metal spots in thin films of solid electrolytes.[15−17]

All these compounds are mainly based on substructures with isolated X^- and Q^{2-} anions, and they therefore have to be regarded as predominantly ionic in character. On the other hand, a reasonable number of copper(I) or silver(I) chalcogen halides with formally neutral and exclusively covalent chalcogen bonds have been found to date. Polymeric chalcogen chains have been observed for MXTe (M = Cu, X = I, Br, Cl; M = Ag, X = I)[18−21] and MXQ_2 (M = Cu, Ag; X = I, Br, Cl; Q = Te, Se),[22−27] whereas six-membered chalcogen rings have been realized in $CuXSe_3$ (X = I, Br)[28−30] and $AgIQ_3$ (with Q = Te, Se).[31,32] Chalcogenide

* To whom correspondence should be addressed. Phone: 49-251-83-36645. Fax: 49-251-83-36002. E-mail: nilges@uni-muenster.de.

(1) Yamashita, T.; Sekid, S. (Matsushita Electric Industrial Co. Ltd., Japan) Patent JP 01039779.
(2) Kozicki, M. N. U.S. Patent 2003107105.
(3) Suzuki, T.; Nishi, Y.; Fujimoto, M.; Awaya, N.; Inoue, T.; Sakiyama, K. (Taiyo Yuden Co. Ltd., Japan; Sharp Corp.) Patent JP 2004273656.
(4) Pan, W.; Wie, H.; Sheng, T.; Zhuang, W.-W. (Sharp Laboratories of America, United States), U.S. Patent 2003197587.
(5) Felser, C.; Block, T. Patent WO 2002069356.
(6) Owens, F. (The United States of America as Represented by the Secretary of the Army) U.S. Patent 6304083.
(7) Reuter, B.; Hardel, K. *Naturwissenschaften* **1961**, *48*, 161.
(8) Reuter, B.; Hardel, K. *Z. Anorg. Allg. Chem.* **1965**, *340*, 168.
(9) Hull, S.; Keen, D. A.; Gardner, N. J. G.; Hayes, W. *J. Phys.: Condens. Matter* **2001**, *13*, 2295.
(10) Blachnik, R.; Dreisbach, H. *J. Solid State Chem.* **1985**, *60*, 115.
(11) Doert, T.; Rönsch, E.; Schnieders, F.; Böttcher, P.; Sieler, J. *Z. Anorg. Allg. Chem.* **2000**, *626*, 89.
(12) Xu, R.; Husmann, A.; Rosenbaum, T. F.; Saboungi, M.-L.; Enderby, J. E.; Littlewood, P. B. *Nature* **1997**, *390*, 57.
(13) Beck, G.; Korte, C.; Janek, J.; Gruhl, F.; von Kreutzbruck, M. *J. Appl. Phys.* **2004**, *96*, 5619.
(14) von Kreutzbruck, M.; Mogwitz, B.; Gruhl, F.; Kienle, L.; Korte, C.; Janek, J. *Appl. Phys. Lett.* **2005**, *86*, 072102.
(15) Kozicki, M. N.; Mitkova, M.; Park, M.; Balakrishnan, M.; Gopalan, C. *Superlattices Microstruct.* **2003**, *34*, 459.
(16) Pinnow, C.-U.; Happ T. (Infineon Technologies AG, Germany) Patent DE 102004014965.
(17) Pinnow, C.-U.; Mikolajick, T.; Happ, T.; Symanczyk, R. (Infineon Technologies AG, Germany) Patent DE 10323414.
(18) Milius, W. *Z. Anorg. Allg. Chem.* **1990**, *586*, 175.
(19) Bachmann, R.; Kreuer, K. D.; Rabenau, A.; Schulz, H. *Acta Crystallogr., Sect. B* **1982**, *38*, 2361.
(20) Fenner, J.; Schulz, H. *Acta Crystallogr., Sect. B* **1979**, *35*, 307.
(21) Schnieders, F.; Böttcher, P. *Z. Kristallogr.* **1995**, *210*, 323.
(22) Fenner, J. *Acta Crystallogr., Sect. B* **1976**, *32*, 3084.
(23) Milius, W. *Z. Naturforsch., B: Chem. Sci.* **1989**, *44*, 990.
(24) Milius, W.; Rabenau, A. *Z. Naturforsch., B: Chem. Sci.* **1988**, *43*, 243.
(25) Pfitzner, A.; Nilges, T.; Deiseroth, H.-J. *Z. Anorg. Allg. Chem.* **1999**, *625*, 201.
(26) Pfitzner, A.; Zimmerer, S. *Z. Anorg. Allg. Chem.* **1995**, *621*, 969.
(27) Pfitzner, A.; Zimmerer, S. *Z. Anorg. Allg. Chem.* **1996**, *622*, 853.
(28) Haendler, H. M.; Carkner, P. M.; Boudreau, S. M.; Boudreau, R. A. *J. Solid State Chem.* **1979**, *29*, 35.
(29) Milius, W.; Rabenau, A. *Mater. Res. Bull.* **1987**, *22*, 1493.
(30) Pfitzner, A.; Zimmerer, S. *Z. Kristallogr.* **1997**, *212*, 203.
(31) Wagener, M.; Deiseroth, H.-J.; Engelen, B.; Reiner, C.; Kong, S. T. *Z. Anorg. Allg. Chem.* **2004**, *630*, 1765.
(32) Deiseroth, H.-J.; Wagener, M.; Neumann, E. *Eur. J. Inorg. Chem.* **2004**, *24*, 4755.

10.1021/cm060226m CCC: $33.50
Published on Web 04/07/2006

substructures with $[Te_2]^{2-}$ dumbbells coordinated in various ways are present in AuITe and $AuITe_2$.[33,34]

Recently, we were able to show that the chalcogenide substructure is the dominant part determining the ion mobility in silver chalcogenide halides.[35−37] Predominantly ionic materials with a high mobile-ion concentration per formula unit are often excellent conductors. In the case of the covalent compounds, the advantage of a low partial charge per chalcogen atom is overcompensated by the low mobile-ion concentration per formula unit, usually resulting in poor conductors. The linkage of the two structure families showing both ionic and partially covalent chalcogen structure motifs, and therefore the combination of the positive aspects for the optimization of ion conduction, is missing completely for any copper, silver, or gold chalcogenide halide.

So far, a structural motif represented by isolated Te^{2-} and covalent $[Te_x]^{2-}$ groups ($x = 2, 3$) is realized for a few binary chalcogenide minerals and substitution variants such as $Ag_{5-x}Te_3$, $Ag_{12}Te_6S$, $AuAgTe_4$, $Au_{0.8}Ag_{0.2}Te_2$, and AgTe.[38−42] S^{2-} and covalent $[S_2]$ dumbbells are reported after the partial electrochemical reduction of sulfur for $Ba_2Ag_8S_7$.[43]

We report on the preparation, crystal structure, and physical properties of the first M(group 11) (poly)chalcogenide halide with both partial covalent and ionic chalcogen structure motifs.

2. Experimental Section

2.1. Synthesis. $Ag_{10}Te_4Br_3$ was prepared from a 7:3:4 mixture of silver (Chempur, 99.9%), silver(I) bromide (Chempur, 99.9%), and tellurium (Alfa Aesar, 99.9999%). The starting materials were sealed into evacuated silica ampules, heated to 1270 K, held at this temperature for 1 day, and quenched in an ice bath. The crude product was finely ground and annealed at 620 K for 3 weeks, followed by a slow cooling to room temperature. This synthesis route leads to phase-pure microcrystalline material. Dark gray single crystals, suitable for structure determination, were isolated from a reaction batch of an 8:1:4 mixture of silver, silver(I) bromide, tellurium, and some additional tellurium(IV)−bromide (50 mg to 1 g of product; Alfa Aesar, 99.9%). Tellurium(IV)−bromide was added to allow mineralization and to increase the crystal growth rate. A transportation of material to the ampule walls was not observed. Crystals were separated directly from the bulk phase. $Ag_{10}Te_4Br_3$ is not light sensitive and is stable in air for several weeks.

2.2. Electron Microprobe Analyses. Semiquantitative analysis was performed with a Leica 420i scanning electron microscope (Zeiss) fitted with an electron dispersive detector unit (Oxford). Silver, HgTe (Te), and KBr (Br) were used as standards for calibration. A voltage of 20 kV was applied to the samples.

(33) Fenner, J.; Mootz, D. *J. Solid State Chem.* **1978**, *24*, 367.
(34) Haendler, H. M.; Mootz, D.; Rabenau, A.; Rosenstein, G. *J. Solid State Chem.* **1974**, *10*, 175.
(35) Nilges, T.; Nilges, S.; Pfitzner, A.; Doert, T.; Böttcher, P. *Chem. Mater.* **2004**, *16*, 806.
(36) Nilges, T.; Dreher, C.; Hezinger, A. *Solid State Sci.* **2005**, *7*, 79.
(37) Nilges, T.; Lange, S. *Z. Anorg. Allg. Chem.* **2005**, *631*, 3002.
(38) Peters, J.; Conrad, O.; Bremer, B.; Krebs, B. *Z. Anorg. Allg. Chem.* **1996**, *622*, 1823.
(39) Deiseroth, H.-J.; Mikus, H. *Z. Anorg. Allg. Chem.* **2005**, *631*, 1233.
(40) Pertlik, F. *Tschermaks Mineral. Petrogr. Mitt.* **1984**, *33*, 203.
(41) Pertlik, F. *Tschermaks Mineral. Petrogr. Mitt.* **1984**, *33*, 253.
(42) Bindi, L.; Spry, P. G.; Cipriani, C. *Am. Mineral.* **2004**, *89*, 1043.
(43) Li, H.; Hwu, S.-J. *Angew. Chem.* **1999**, *111*, 3253; *Angew. Chem., Int. Ed.* **1999**, *38*, 3067.

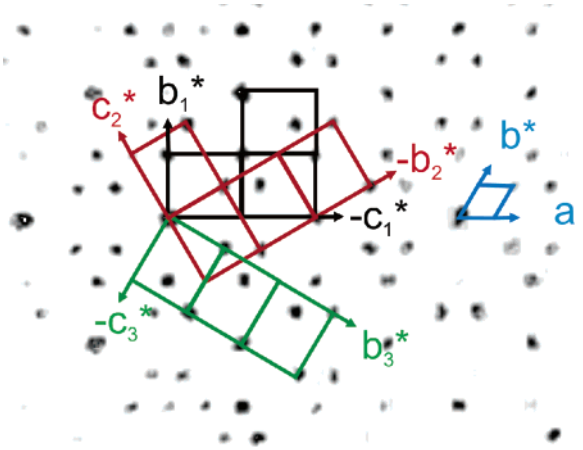

Figure 1. Projection of four precession photographs (*hk*0 to *hk*4) of $Ag_{10}Te_4Br_3$. The hexagonal pseudocell (blue) and the three twin domains (black, red, green) are drawn.

2.3. XRD Experiments. Phase analysis was done by X-ray powder diffraction of finely ground samples using a Stoe StadiP X-ray powder diffractometer operated with Cu $K_{\alpha 1}$ radiation (λ = 1.54051 Å) and equipped with a linear 5° PSD (Braun). Silicon was used as an external standard. Diffractograms were recorded in a transmission setup at 298 K within the 2θ range 6−100°.

Intensity data of two different systematically twinned crystals (crystal 1 and crystal 2) from independent batches were collected on a Stoe-IPDS II-Image plate diffractometer fitted with Mo K_α radiation (λ = 0.71073 Å). The datasets were corrected from Lorentz and polarization effects.

2.4. Raman Spectroscopy. Raman spectra were recorded at 121 K by using a Bruker RFS100/S-FT Raman spectrometer in backscattering mode fitted with a Nd:YAG laser (λ = 1064 nm). A resolution of ±2 cm^{-1} has to be estimated for the measurements. A finely ground sample was transferred to a glass capillary of 0.3 mm inner diameter and sealed prior to the measurement. To avoid thermal decomposition during the measurement, we applied only a small laser powder of 1 mV and accumulated a total number of 1000 scans.

2.5. Impedance Spectroscopy. AC conductivity measurements were performed using a Novocontrol alpha-S impedance analyzer applying a frequency range of 10 mHz to 3 MHz and a temperature range of 153 to 293 K. Ion-blocking gold electrodes were sputtered (Baltec SCD 005) on a cold pressed pellet of finely ground $Ag_{10}Te_4Br_3$, and the sample was fitted to a Novocontrol standard sample cell BDS 1200. Impedance spectra were recorded under an oxygen and moisture-free nitrogen atmosphere applying an equilibration time of 1−5 min between each measurement after reaching the measurement temperature.

3. Results

3.1. Structure Refinement of $Ag_{10}Te_4Br_3$. A careful investigation of precession photographs of two different crystals revealed systematic twinning (three twin domains). The twin domains were derived from a primitive pseudo-hexagonal cell of lattice constants a = 31.544(2) Å, c = 15.374(1) Å, and V = 13285(1) $Å^3$ using the transformation matrices (by rows) T_1 = (0 0 1 $^1/_2$ 0 0 $^1/_4$ $^1/_2$ 0), T_2 = (0 0 1 0 $-^1/_2$ 0 $^1/_2$ $^1/_4$ 0), and T_3 = (0 0 1 $^1/_2$ $^1/_2$ 0 $-^1/_4$ $^1/_4$ 0). Crystals with twin ratios of 0.347(1):0.315(1):0.338(1) (crystal 1) and 0.909(1):0.072(1):0.018(1) (crystal 2) were investigated by single-crystal X-ray diffraction experiments. Because of the significantly better crystal quality of crystal

Table 1. Crystallographic Data of $Ag_{10}Te_4Br_3$

empirical formula	$Ag_{10}Te_4Br_3$[a]
fw	1828.8
cryst shape and color	isomorphic, dark gray
cryst size (mm^3)	0.07 × 0.06 × 0.06
cryst syst	orthorhombic
space group	*Cmcm* (No. 63)
Z	8
a (Å)	15.374(1)
b (Å)	15.772(1)
c (Å)	13.715(1)
V ($Å^3$)	3325.6(4)
T (K)	293
F(000)	6264
ρ_{calcd} (g cm^{-3})	7.303
no. of reflns	27 330
twin matrices (by rows)	$T_{1/2}$ (1 0 0 0 $^1/_2$ $^3/_4$ 0 −1 $^1/_2$); $T_{1/3}$ (1 0 0 0 $^1/_2$ $^{-3}/_4$ 0 1 $^1/_2$)
refinement method	full-matrix least-squares twin (*hklf* 5) refinement on F^2 [45]
$R_{\sigma I}$	0.1096
params	159
final R values [$I > 3\sigma_I$] R1	0.0605
wR2	0.0792
final R values (all) R1	0.2211
wR2	0.0936
largest difference peak and hole (e $Å^{-3}$)	2.41/−1.80

[a] CSD-416031 contains the supplementary crystallographic data for this twin refinement. These data can be obtained free of charge from the Fachinformationzentrum Karlsruhe, D-76344 Leopoldshafen (fax: 49 7247-808-666; e-mail: crysdata@fiz-karlsruhe.de) on request.

Table 2. Atomic Coordinates and Isotropic Displacement Parameters ($Å^2$) for $Ag_{10}Te_4Br_3$

atom	Wyckoff position	occupancy (%)	*x*	*y*	*z*	U_{iso}
Te1	8*g*	100	0.32519(2)	0.62592(3)	$^1/_4$	0.0223(1)
Te2	8*g*	100	0.40884(2)	0.11993(3)	$^1/_4$	0.0337(1)
Te3	8*f*	100	$^1/_2$	0.37793(4)	0.08805(3)	0.0369(1)
Te4	8*f*	100	$^1/_2$	0.87500(4)	0.05313(4)	0.0368(1)
Br1	8*e*	100	0.24961(4)	0	0	0.0372(3)
Br2	8*d*	100	$^1/_4$	$^1/_4$	$^1/_2$	0.0407(3)
Br3	8*g*	100	0.25718(4)	0.37229(6)	$^1/_4$	0.0364(2)
Ag1	4*c*	100	$^1/_2$	0.64572(7)	$^1/_4$	0.0674(4)
Ag2	4*c*	100	$^1/_2$	0.8820(2)	$^1/_4$	0.0548(3)
Ag3	16*h*	100	0.3727(1)	0.9781(1)	0.1351(1)	0.1014(3)
Ag4	16*h*	100	0.38923(8)	0.75997(8)	0.1350(1)	0.0898(3)
Ag5	8*g*	100	0.4060(1)	0.47015(6)	$^1/_4$	0.1327(6)
Ag6	16*h*	100	0.4004(1)	0.5820(2)	0.0714(1)	0.1564(5)
Ag7a	16*h*	50	0.3877(2)	0.2147(2)	0.3999(3)	0.174(1)
Ag7b	16*h*	50	0.3819(2)	0.2706(2)	0.3632(4)	0.114(1)

2, the ongoing discussion is on the basis of results of crystal 2. The space group *Cmcm* (lattice parameters of 15.374(1) Å, $b = 15.772(1)$ Å, $c = 13.715(1)$ Å, and $V = 3325.6(4)$ $Å^3$) could be obtained from systematic extinctions, and the structure was solved using the major twin domain of crystal 2.[44] Figure 1 illustrates the systematic twinning occurring in $Ag_{10}Te_4Br_3$.

A twin refinement of a complete dataset applying a nonharmonic refinement up to 3rd order terms for all silver positions resulted in final R values of R1 = 0.0605 wR2 = 0.0792 for reflections with $I > 3\sigma_I$ and R1 = 0.2218, wR2 = 0.0936 for all reflections.[45] All atomic positions have been refined applying a full occupancy, except for Ag7. Because of large displacement parameters for this position, a better

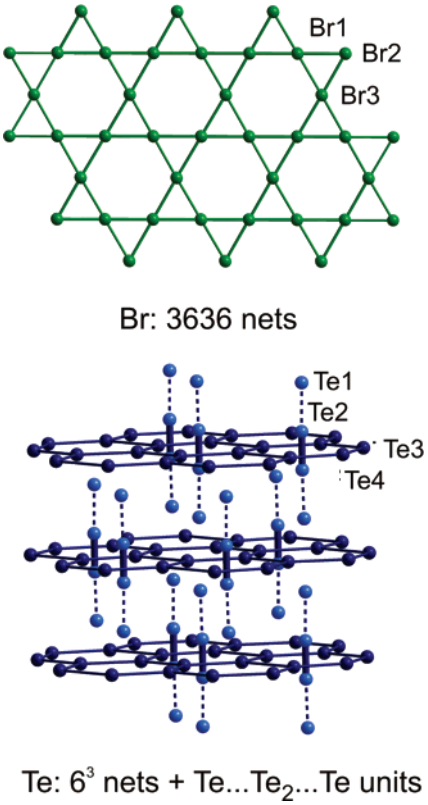

Figure 2. Anion substructures in $Ag_{10}Te_4Br_3$. Slightly distorted 3636 Br nets (green spheres) and 6^3 Te nets (dark blue spheres) are stacked along the *a* axis. Predominantly covalent units formed by $[Te_2]^{2-}$ dumbbells and two additional Te positions (light blue spheres) are centering half of the six-membered rings of the tellurium 6^3 nets.

description of the silver distribution was achieved by a split into two half-occupied sites in the final refinement steps. Crystallographic data are summarized in Tables 1 and 2. A brief description of the refinement strategy used for solid electrolytes[35] and the nonharmonic refinements[46−49] is given elsewhere. The nonharmonic description of the silver displacement did significantly improve the structure model. To check the relevance and significance of the 3rd order terms, we performed a careful analysis of the resulting joint probability density functions (jpdf). We found no more-negative jpdf regions than 2% of the maximum of the positive jpdf. A reflection:parameter ratio of approximately 100:1 is sufficient to derive reliable information. The high R1 value for all data of the twin refinement is due to the low scattering power of the minority twin fractions.

3.2. Structure Description. $Ag_{10}Te_4Br_3$ consists of two characteristic anion networks that are slightly distorted Kagomé nets of Br^- and 6^3 nets of Te^{2-} ions. The tellurium nets are comparable with the AlB_2 type boron substructure, also realized in the superconductor MgB_2 (Figures 2 and 3).[50−52]

The very narrow Br−Br distance distribution from 3.936(1) to 3.978(1) Å substantiates the almost-ideal character of

(44) Sheldrick, G. M. *SHELXS97*; University of Göttingen: Göttingen, Germany, 1997.
(45) Petricek, V.; Dusek, M.; Palatinus, L. *JANA2000, The Crystallographic Computing System*; Institute of Physics: Praha, Czech Republic, 2000.
(46) Kuhs, W. F. *Acta Crystallogr., Sect. A* **1992**, *48*, 80.
(47) Willis, B. T. M. *Acta Crystallogr., Sect. A* **1969**, *25*, 277.
(48) Bachmann, R.; Schulz, H. *Acta Crystallogr., Sect. A* **1984**, *40*, 668.
(49) Zucker, U. H.; Schulz, H. *Acta Crystallogr., Sect. A* **1982**, *38*, 563.
(50) Hofmann, W.; Jänische, W. *Naturwissenschaften* **1935**, *23*, 851.
(51) Jones, M. E.; Marsh, R. E. *J. Am. Chem. Soc.* **1954**, *76*, 1434.
(52) Nagamatshu, J.; Nakagawa, N.; Muranaka, T.; Zenitani, Y.; Akimitsu, J. *Nature* **2001**, *410*, 63.

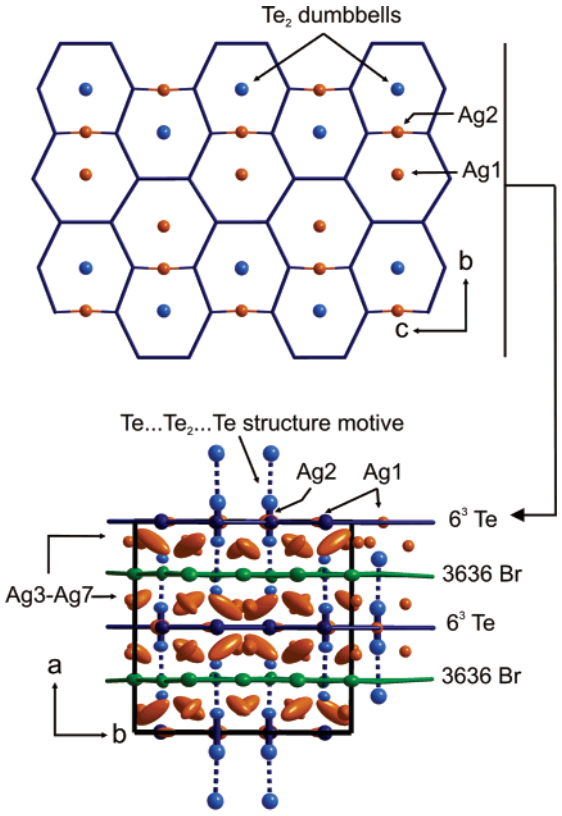

Figure 3. Silver distribution in $Ag_{10}Te_4Br_3$. Top: distorted 6^3 Te nets with $[Te_2]^{2-}$ dumbbells and Ag1 centring the tellurium hexagons. Ag2 is linearly coordinated by tellurium. Bottom: distribution of the Ag3 to Ag7a,b positions on distinct silver layers parallel to the tellurium and bromine nets. A 90% probability level of displacement parameters is drawn for all atoms within the unit cell (black line).

the Kagomé net. Only a very slight deviation from planarity can be observed, resulting in torsion angles of not more than 3.54(1)° within the six-membered rings.

$[Te_2]^{2-}$ dumbbells (Te2) center half of the hexagonal tellurium rings (Te3 and Te4, d(Te3−Te4) from 4.204(1) to 5.400(1) Å) of the 6^3 nets (see Figure 2). A bond distance of 2.803(1) Å is typical for a single bond, slightly shorter than in elemental tellurium and comparable with a 2.79 Å average distance of $[Te_2]^{2-}$ dumbbells reported in the literature.[53−56] The zigzaglike ordering principle of the tellurium dumbbells relative to the 6^3 net along the c axis can be easily derived from Figure 3. The $[Te_2]^{2-}$ dumbbells are neighbored by additional tellurium positions (d(Te1−Te2) = 3.599(1) Å). The distance lies well below 4.12 Å, which represents two times the van der Waals radius of Te^{2-} ions, according to Pauling.[57] Compared with the dispersion interactions in $CrTe_3$, $ZrTe_3$ (d(Te···Te) = 3.51−3.70 Å),[58,59] and elemental tellurium (d(Te···Te) = 3.458 Å),[60] the present distance is located within a comparable range (see Table 3). Distances of d(Te2−Te4) = 4.388(1) Å and d(Te2−Te3) = 4.843(1) Å are the closest ones between the $[Te_2]^{2-}$ dumbbells and the 6^3 nets. Te1−Te3/Te4 distances are well above 5 Å.

Table 3. Selected Interatomic Distances (Å) in $Ag_{10}Te_4Br_3$

atom 1	atom 2	d (Å)	atom 1	atom 2	*d* (Å)
Te1	Ag1 (1×)	2.7056(4)	Ag1	Ag4 (4×)	2.938(2)
	Ag4 (2×)	2.815(1)		Ag6 (4×)	3.059(2)
	Ag5 (1×)	2.753(1)	Ag2	Ag3 (4×)	2.934(2)
	Ag6 (2×)	2.796(2)		Ag4 (4×)	3.015(2)
Te2	Te2 (1×)	2.8030(5)	Ag3	Ag2 (1×)	2.934(2)
	Ag3 (2×)	2.793(2)	Ag4	Ag1 (1×)	2.938(2)
	Ag7a (2×)	2.562(4)		Ag2 (1×)	3.015(2)
	Ag7b (2×)	2.869(4)		Ag6 (1×)	2.945(3)
Te3	Ag5 (2×)	3.023(1)	Ag5	Ag5 (1×)	2.890(2)
	Ag6 (2×)	2.744(2)		Ag6 (2×)	3.020(2)
	Ag7b (2×)	2.571(3)	Ag6	Ag1 (1×)	3.059(2)
Te4	Ag2 (1×)	2.7024(6)		Ag4 (1×)	2.945(3)
	Ag3 (2×)	2.782(2)		Ag5 (1×)	3.020(2)
	Ag4 (2×)	2.730(1)		Ag6 (1×)	3.064(3)
	Ag7a (2×)	3.066(4)	Ag7a[a]	Ag7b[a] (1×)	1.020(5)
Br1	Ag3 (2×)	2.671(2)	Br3	Ag3 (2×)	3.042(2)
	Ag6 (2×)	2.819(2)		Ag5 (1×)	2.760(2)
Br2	Ag4 (2×)	2.835(1)		Ag7b (2×)	2.943(4)
	Ag7a (2×)	2.584(3)			
	Ag7b (2×)	2.782(4)			

[a] Occupancy 50%.

Two sets of silver positions can be differentiated from a structure chemical point of view and by taking topological considerations into account. Figure 3 illustrates the silver distribution within the anion substructure. Ag1 and Ag2 are both localized within the 6^3 tellurium nets. Ag1 centers the hexagons of the 6^3 Te nets (d(Ag−Te) > 4.5 Å) not occupied by a $[Te_2]^{2-}$ dumbbell, whereas Ag2 is linearly coordinated by the telluride ions with distances of 2.702(1) Å. Eight of the 10 silver atoms per formula unit (Ag3−Ag7) are located on distinct silver layers between the tellurium and the bromine nets, directly neighboring the predominantly covalent chalcogen units. A detailed description of the silver distribution is given in chapter 4.2, where the silver mobility of $Ag_{10}Te_4Br_3$ is discussed.

3.2. Phase Analytical Results. Phase analysis was done by X-ray powder diffraction and semiquantitative EDX measurements. The X-ray powder patterns showed no other reflections except those for $Ag_{10}Te_4Br_3$. All reflections could be indexed and refined using an orthorhombic C-centered cell with lattice parameters a = 15.367(3) Å, b = 15.793(4) Å, c = 13.727(4) Å, and V = 3331(2) Å^3. Those values are in good agreement with the data derived from single-crystal X-ray diffraction (Figure 4).

Semiquantitative EDX measurements were performed from the single crystals used for structure determination. Values of Ag 56(2) (*58.9*), Te 24(2) (*23.5*), and Br 20(2) (*17.6*), in at %, were averaged from three to five different measurements of each crystal. Estimated standard deviations are given in parentheses and theoretical values in italics. The small discrepancies in the EDX data are due to the irregular surface of the single crystals.

3.3. Impedance Spectroscopy. The total conductivity of $Ag_{10}Te_4Br_3$ was determined from temperature-dependent impedance spectroscopic measurements between 153 and 293 K. Nyquist plots showed the typical behavior of an ion-

(53) Bensch, W.; Dürichen, P. *Acta Crystallogr., Sect. C* **1997**, *53*, 267.
(54) Assoud, A.; Derakhshan, S.; Soheilnia, N.; Kleinke, H. *Chem. Mater.* **2004**, *16*, 4193.
(55) Chen, X.; Huang, X.; Li, J. *Inorg. Chem.* **2001**, *40*, 1341.
(56) Huang, S. D.; Lai, C. P.; Barnes, C. L. *Angew. Chem.* **1997**, *109*, 1961.; *Angew. Chem., Int. Ed.* **1997**, *36*, 1854.
(57) Pauling, L. *The Nature of the Chemical Bond*; Cornell University Press: Ithaca, NY, 1945.
(58) Canadell, E.; Jobic, S.; Brec, R.; Rouxel, J. *J. Solid State Chem.* **1992**, *98*, 59.
(59) Stöwe, K.; Wagner, F. *J. Solid State Chem.* **1998**, *138*, 160.
(60) Bradley, A. J. *Philos. Mag.* **1924**, *48*, 477.

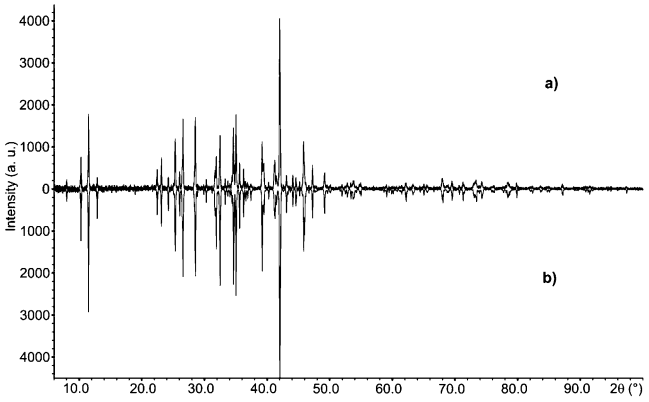

Figure 4. Comparison of (a) measured and (b) calculated X-ray powder diffractogram of $Ag_{10}Te_4Br_3$. The calculated pattern is drawn with intensities pointing down for better comparison. Lattice parameters for (a) are $a = 15.367(3)$, $b = 15.793(4)$, $c = 13.727(4)$ Å, and $V = 3331(2)$ Å^3; those for the calculated pattern (b) are based on the single-crystal structure data: space group *Cmcm*, $a = 15.374(1)$, $b = 15.772(1)$, $c = 13.715(1)$ Å, and $V = 3325.6(4)$ Å^3.

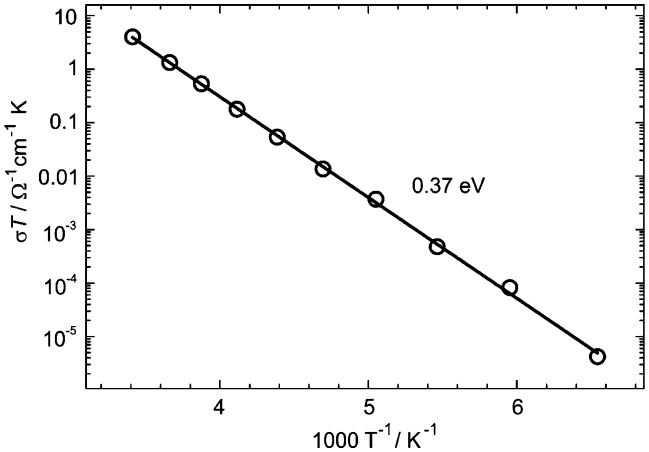

Figure 5. Arrhenius plot of the total conductivity of $Ag_{10}Te_4Br_3$.

conducting material, which includes a semicircle at high frequencies and a linear spike at low frequencies. Figure 5 illustrates the temperature-dependent total conductivity of $Ag_{10}Te_4Br_3$. On plotting the conductivity against the reciprocal temperature, one can observe a linear trend pointing toward an Arrhenius-like behavior of $Ag_{10}Te_4Br_3$. It has to be stated at this stage that the electronic counterpart of the total conductivity has not been determined yet, but a predominantly ionic conductivity can be concluded from the impedance spectroscopic results. Suitable experiments are currently underway and will be reported soon.

Conductivities of $\sigma = 1.4 \times 10^{-2}\ \Omega^{-1}\ cm^{-1}$ at 293 K and $\sigma = 2.8 \times 10^{-8}\ \Omega^{-1}\ cm^{-1}$ at 153 K were found. Those values at room temperature are on the same order of magnitude compared with other crystalline silver-ion conductors such as β-Ag_3SI or $Ag_7I_4PO_4$ and only 1 order of magnitude smaller than the best-known crystalline silver-ion conductor, $RbAg_4I_5$. Table 4 gives an overview of the conductivities of different crystalline and glassy electrolytes reported in the literature for comparison.

3.4. Raman Spectroscopy. The occurrence of a $[Te_2]^{2-}$ dumbbell in $Ag_{10}Te_4Br_3$ was substantiated by Raman spectroscopy. A single band was observed at 168 cm^{-1}, which is in good agreement with the frequencies previously assigned for tellurium−tellurium modes (298 K) found in elemental tellurium, polytellurides, and free polytelluride complexes. Examples are 170 cm^{-1} for Te, 160 and 173 cm^{-1} for $[Cd_4Te_{12}]^{4-}$ and $[Hg_4Te_{12}]$,$^{4-}$ 219 and 188 cm^{-1} for $[Te_4]^{2-}$, and 200 cm^{-1} for $[PdTe_8]^{2-}$.[73−76]

Table 4. Conductivities of Crystalline and Glassy Silver-Ion Conductors

	σ (Ω^{-1} cm^{-1})	T (K)	ref
crystalline compds			
$RbAg_4I_5$	2.1×10^{-1}	295	61
KAg_4I_4CN	1.4×10^{-1}	298	62
$Ag_{2.0}Hg_{0.25}S_{0.5}I_{1.5}$	1.4×10^{-1}	298	63
$Ag_7I_4PO_4$	1.9×10^{-2}	298	64
$Ag_{10}Te_4Br_3$	1.4×10^{-2}	293	this work
β-Ag_3SI	1.0×10^{-2}	298	65
β-Ag_3SBr	$\sim 5 \times 10^{-3}$	298	66
AgBr	$\sim 1 \times 10^{-6}$	298	67
glassy materials			
$45GeS_2-55Ag_2S$	1.4×10^{-3}	298	68
35AgCl-45AgI-20CsCl	4.7×10^{-2}	298	69, 70
$AgI-Ag_2Se-P_2Se_5$	$\sim 1 \times 10^{-2}$	298	71, 72

4. Discussion

4.1. Crystal Chemistry. The crystal structure of $Ag_{10}Te_4Br_3$ was successfully determined by single-crystal X-ray diffraction from systematically twinned crystals. Semiquantitative EDX measurements of the single crystals used for structure determination confirmed the composition derived after structure determination. $Ag_{10}Te_4Br_3$ is the first example of an M(group 11) (poly)chalcogenide halide with Te−Te interactions. A summary of the known ternary M(group 11) (poly)chalcogenide halides is given in the Supporting Information. Counting silver as Ag^+, bromine as Br^-, and the Te_2 group as $[Te_2]^{2-}$, one obtains the formula $(Ag^+)_{10}(Te_2^{2-})_{0.5}(Te^{2-})_3(Br^-)_3$. The occurrence of attractive tellurium interactions is caused by the higher tendency of tellurium to form Te−Te bonds compared with the lighter chalcogen homologues.[77] Focusing on the cation/anion ratio of 1.43 and on the non-tellurium:tellurium ratio of 3.25, we do not generally expect the existence of Te−Te interactions. The lower the ratio, the more tellurium tends to form Te−Te interactions. A high ratio can only be observed if tellurium functions as a complex ligand in metal telluride

(61) Bradley J. N.; Greene, P. D. *Trans. Faraday Soc.* **1967**, *63*, 424.
(62) Mellors G. W.; Luzos, D. V. *J. Electrochem. Soc.* **1975**, *118*, 846.
(63) Takahashi, T. *J. Appl. Electrochem.* **1973**, *3*, 79.
(64) Takahashi, T.; Ikeda, S.; Yamamoto, O. *J. Electrochem. Soc.* **1972**, *119*, 477.
(65) Reuter, B.; Hardel, K. *Ber. Bunsen-Ges. Phys. Chem.* **1966**, *70*, 82.
(66) Kawamura, J.; Shimoji, M. *Solid State Ionics* **1981**, *3/4*, 41.
(67) Maier, J. *Mater. Res. Bull.* **1985**, *20*, 383.
(68) Robinel, E.; Carette, B.; Ribes, M. *J. Non-Cryst. Solids* **1983**, *57*, 49.
(69) Liu, C.; Sundar, H. G. K.; Angell, C. A. *Mater. Res. Bull.* **1985**, *20*, 525.
(70) Liu, C.; Sundar, H. G. K.; Angell, C. A. *Solid State Ionics* **1986**, *18/19*, 442.
(71) Minami, T. *J. Non-Cryst. Solids* **1983**, *56*, 15.
(72) Minami, T. *J. Non-Cryst. Solids* **1985**, *73*, 293.
(73) Weidlein, J.; Müller, U.; Dehnicke, K. *Schwingungsspektroskopie*; Georg Thieme: Stuttgart, Germany, 1982; pp 27, 46, and 103.
(74) Kim, K.-W.; Kanatzidis, M. G. *Inorg. Chim. Acta* **1994**, *224*, 163.
(75) Wolkers, H.; Schreiner, B.; Staffel, R.; Müller, U.; Dehnicke, K. *Z. Naturforsch., B: Chem. Sci.* **1991**, *46*, 1015.
(76) Wolkers, H.; Dehnicke, K.; Fenske, D.; Khassanov, A.; Hafner, S. S. *Acta Crystallogr., Sect. C* **1991**, *47*, 1627.
(77) Tremel, W. *Angew. Chem.* **1991**, *103*, 900; *Angew. Chem., Int. Ed.* **1991**, *30*, 840.

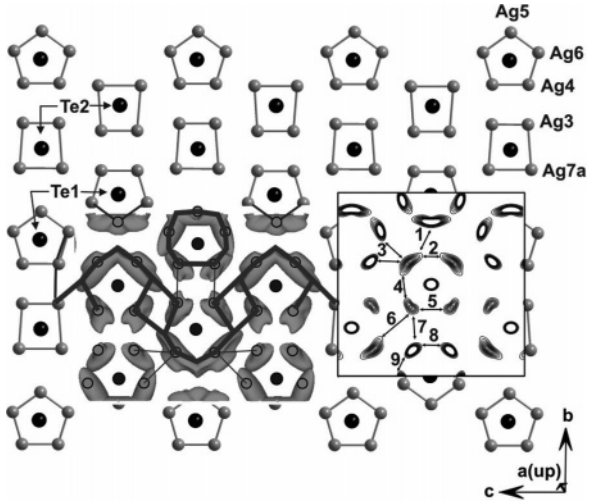

Figure 6. Silver distribution (Ag3−Ag7a) within the silver layer in $Ag_{10}Te_4Br_3$. The dark gray lines represent the first coordination sphere around the covalently bonded Te1 and Te2 positions. Joint probability density functions are drawn at a 0.9999 isovalue to illustrate the preferred diffusion pathways of silver around the Te_2 dumbbells (Te2) and around the Te1 position. Contour lines are at 0.1 $Å^{-3}$. Maximum pdf = 6.87, minimum pdf = −0.04 $Å^{-3}$. The negative pdf is not drawn for clarity. One-particle potentials calculated from a jpdf map between the areas of high probability density at the coordinate $x = 0.1$ substantiate the postulated pathways. Selected opp values (eV): 1, >0.9; 2, 0.20; 3, >0.9; 4, 0.35; 5, 0.51; 6, 0.45; 7, 0.70; 8, 0.40; 9, 0.28. Big solid lines indicate the low potential pathways within the silver layer, whereas small solid lines symbolize the areas of high potential.

clusters such as niobocene derivates (e.g., R_2NbTe_2H, R = cyclopentadienlye) or if formal neutral ligands such as CO in $[Ru_2(Te_2)_7(CO)_{12}]^{2-}$ or $[Fe_2Te_3(CO)_{12}]^{2-}$ are involved in the coordination chemistry of the materials.[78,56,79−81] K_5Te_3 (ratio 1.67), $Ag_{4.53}Te_3$ (ratio 1.51), and $Ag_{12}Te_6S$ (1.17 cation: anion ratio; 2.17 non-tellurium:tellurium ratio) are some of the rare "saltlike" inorganic materials that show Te−Te interactions with cation:anion and non-tellurium:tellurium ratios greater than 1.[82,38,39]

4.2. Ion Dynamics in $Ag_{10}Te_4Br_3$. One outstanding property of $Ag_{10}Te_4Br_3$ is the anisotropic silver mobility within the silver layers. From a topological point of view, an interesting arrangement of four- (d(Ag−Ag) = 3.152(2)−4.112(6) Å) and five-membered (d(Ag−Ag) = 2.945(3) − 3.153(2) Å) ring units can be observed for the Ag3−Ag7a,b positions (Figure 6).

The four-membered unit (Ag3, Ag7a,b) is located in the direct neighborhood of the predominantly covalent Te_4 structural motif represented by the Te1 and Te2 positions. Joint probability density function (jpdf) analysis of silver in both structure sections was performed, and a high silver mobility can be derived from the shape of the probability density within the silver layers. The strong nonharmonicity within the five-membered unit on the one hand and within and between the four-membered units on the other hand points toward a somewhat different diffusion tendency of silver in the layer. Preferred diffusion pathways can be predicted from the analysis of the one-particle potentials (opp). Low potentials up to a maximum of 0.40 eV have been found within the five-membered ring arrangement located around the Te1 position. A 1D diffusion pathway with only slightly higher potentials can be derived from the opp's along the positions of the four-membered units with a maximum of 0.45 eV between the Ag3 and Ag7 positions of adjacent units (see Figure 6 and Table 5). Obviously, the lowest potential (0.20 eV) and therefore the highest silver mobility is present between the Ag7 positions in direct neighborhood to the $[Te_2]^{2-}$ dumbbell (Te2).

Table 5. Selected One-Particle Potentials (opp) along the Diffusion Pathways of Silver Ions according to Figure 6 in $Ag_{10}Te_4Br_3$[a]

M1−M2	opp (eV)	structure unit	no. in Figure 6
Ag3−Ag4	0.70	four ↔ five	7
Ag3−Ag7a,b	0.45	four ↔ five	6
Ag4−Ag7a,b	>0.9	four ↔ five	3
Ag5−Ag7a,b	>0.9	four ↔ five	1
Ag6−Ag7a,b	>0.9	four ↔ five	3
Ag4−Ag4	0.40	within five	8
Ag4−Ag6	0.28	within five	9
Ag5−Ag6	<0.1	within five	
Ag3−Ag3	0.51	within four	5
Ag3−Ag7a,b	0.35	within four	4
Ag7−Ag7a,b	0.20	within four	2
	0.37	impedance spectroscopic result	

[a] Potentials are given within and between the four- (Ag3 and Ag7a,7b) and five-membered (Ag4−Ag6) silver units.The activation energy derived from impedance spectroscopic experiments and the lowest potential are marked for comparison.

Opp's between the linearly coordinated silver within the tellurium nets and the neighboring silver layers are in the 0.55−0.78 eV range. These values can be interpreted in terms of a lower ion mobility and diffusion tendency perpendicular to the silver layers. Impedance spectroscopic measurements of powdered samples revealed a high total conductivity and an activation energy of 0.37 eV, in reasonably good agreement with the calculated value derived from the jpdf analysis. The development of further pathways leading to a 2D diffusion of silver can be expected from the shape of the jpdf between Ag7 and Ag4/Ag6 and between Ag3 and Ag4 perpendicular to the 1D pathway.

To realize a 3D ion diffusion, we must transport silver through the bromine nets. No evidence from jpdf analyses was found for a diffusion tendency of silver through the bromine substructure.

5. Conclusion

$Ag_{10}Te_4Br_3$ represents the first ternary M(group11) metal (poly)chalcogenide halide with a high 1D silver mobility within silver layers. The regions of high silver mobility are determined by the covalent tellurium units within the anion substructure, whereas no significant silver dynamic was observed perpendicular to the silver diffusion layers. Layers of bromide ions are separating the structure sections with high ion dynamics. It will be a challenge in the future to verify whether other combinations of covalent tellurium units

(78) Wachter, J. *Eur. J. Inorg. Chem.* **2004**, 1367.
(79) Huang, S.-P.; Kanatzidis, M. G. *J. Am. Chem. Soc.* **1992**, *114*, 5477.
(80) Huang, S.-P.; Kanatzidis, M. G. *Inorg. Chem.* **1993**, *32*, 821.
(81) Eichhorn, B. W.; Haushalter, R. C.; Merola, J. S. *Inorg. Chem.* **1990**, *29*, 728.
(82) Schewe, I.; Böttcher, P. *Z. Naturforsch., B: Chem. Sci.* **1990**, *45*, 417.

with higher condensation grades can also be stabilized together with divalent telluride anions. Promising first experiments are pointing toward new compounds to be explored. A variation in the content and type of the covalently bonded chalcogenide compared with the ionic chalcogenide will give the opportunity to modulate the conduction pathways and to design suitable materials for electronic devices. Also, the transformation of the developed synthetic routes to lighter chalcogen homologues will be of interest because of the fact that covalent interactions become more unexpected. The preparative route of a partial reduction of sulfur by electrochemical methods leading to the formation of $Ba_2Ag_8S_7$ is aided by the thermodynamically controlled partial reduction of tellurium followed by the tellurium-halide-promoted crystallization of $Ag_{10}Te_4Br_3$.

Acknowledgment. The work with the scanning electron microscope by H.-J. Göcke and preparative help by M. Bawohl are gratefully acknowledged. We thank Dr. R.-D. Hoffmann for fruitful discussions, Dr. D. Wilmer and Dr. H.-W. Meyer for the ac conductivity measurements, and Prof. C. Wickleder and R. Stötzel for the preparation of the Raman spectra. This work was financially supported by the Deutsche Forschungsgemeinschaft through SFB 458 "Ionenbewegung in Materialien mit ungeordneten Strukturen."

Supporting Information Available: An overview on existing M(group 11)−chalcogen−halogen compounds and anisotropic displacement parameters of $Ag_{10}Te_4Br_3$. This material is available free of charge via the Internet at http://pubs.acs.org.

CM060226M